Dynamic performance investigation of a Spar-type floating wind turbine in different sea conditions using numerical method and experimental validations

WANG Han[1,2], HU Zhi-qiang[3], MENG Xiang-yin[3]

（1. State Key Laboratory of Ocean Engineering，Shanghai Jiao Tong University，Shanghai 200240，China; 2. Collaborative Innovation Center for Advanced Ship and Deep－Sea Exploration，Shanghai 200240，China; 3. School of Engineering，Newcastle University，Newcastle upon Tyne，NE1 7RU UK）

Abstract: Both numerical calculation and model test are important techniques to study and forecast dynamic response of floating offshore wind turbine (FOWT). However, both the analysis methods have their own limitations at present. In this work, the dynamic responses of a 5 MW OC3 spar-type floating wind turbine designed for a water depth of 200 m are numerically investigated and validated by a 1:50 scaled model test. Most importantly, the discrepancies between numerical calculations and model tests are compared and discussed. According to the comparisons, it can be found that surge and pitch are coupled with mooring tension, but heave is independent from them. Surge and pitch are mainly induced by wave in wind-wave conditions. Wind and current will induce the low-frequency average responses, while wave will induce the fluctuation amplitudes of responses. In addition, wave will induce wave-frequency responses but wind and current will restrain the amplitudes of the responses.

Keywords: spar-type floating wind turbine; dynamic response; numerical calculation; model test; time domain analysis; frequency domain analysis

1. Introduction

With the traditional energy is increasingly exhausted over the past decade, clean and environmental friendly renewable energy, especially offshore wind energy, has attracted more attention than ever before. Nowadays, there have been many of fixed-bottom offshore wind turbines. However, they are restricted to further development due to complaints of noise pollution and unstable power supply. Besides, for the increasing water depth and the rapid growth in economic costs, offshore floating wind turbine is hoped to replace fixed-bottom offshore wind turbine and dominate the development of offshore wind power in future. Nevertheless, the dynamic responses of floating wind turbines are more complex than those of fixed-bottom ones because they will suffer from wind, wave, current and complicated motion responses. Thus, it has important engineering application value to choose appropriate methods to study dynamic responses of floating wind turbines.

Recently, a great deal of research works and concepts of floating offshore wind turbine (FOWT) have been carried out by many scholars all over the world. A 5 MW baseline wind turbine was developed in National Renewable Energy Laboratory (NREL) (Jonkman et al., 2009a). In phase Ⅳ of the Offshore Code Comparison Collaboration (OC3), a spar floating platform which is called OC3-Hywind was designed for the 5MW baseline wind turbine (Jonkman, 2010). In phase Ⅱ of the Offshore Code Comparison Collaboration Continuation (OC4), a semi-type platform was also designed (Robertson et al., 2014). In 2013, a combination of a spar-type floating wind turbine and a floating wave energy converter, i.e. a new concept called Spar Tours Combination (STC) was proposed in NTNU (Muliawan et al., 2013).

In order to verify the dynamic properties of the above concept models, many scholars have developed several simulation codes. Adding the module of HydroDyn and mooring to fixed wind turbine analysis code - Fatigue, Aerodynamics, Structures, and Turbulence (FAST), a fully coupled aero-hydro-servo-elastic simulation tool was developed (Jonkman, 2007). Then, the dynamic responses of OC3-Hywind in different sea conditions were calculated by FAST and other six codes, such as HAWC2, 3Dfloat and Simo (Jonkman et al., 2010). The dynamic responses of OC3-Hywind were also calculated by HAWC2-DeepC (Karimirad et al., 2012) and HydroD-DeepC-TDHMILL3d (Thomas, 2010). SIMO/RIFLEX and AeroDyn were combined to study the coupled dynamic response of WindFloat semi-type platform (Kvittem et al., 2012). MLTSIM-FAST code was developed to calculate the TLP floating wind turbine in DeepCwind Project (Koo et al., 2013). A coupled time domain simulation code - DARwind which considers the high-order rigid - flexible coupled term in multi-body model was developed (Chen et al., 2017).

However, single numerical analysis method cannot fully verify the results. Model test is another method for analyzing dynamic responses and also validate numerical analysis code. In 2006, a 1: 47 scaled model test of Hywind was conducted at Marintek (Nielsen et al., 2006). University of Maine used to unite MARIN to organize

1: 50 scaled model tests of spar, semi and TLP floating platforms to verify the dynamic responses of these three floating wind turbine concepts (Martin et al., 2012; Koo et al., 2012; Goupee et al., 2012; Kimball et al., 2012). In 2004, thrust-matched blade system was developed by MARIN and a new MARIN Stock Wind Turbine (MSWT) model was also proposed (Ridder et al., 2014). Then, the MSWT model was tested by a 1:130 scaled model in University of Maine (Kimball et al., 2014). A 1:100 scaled model test was conducted to verify the dynamic response of a spar floating wind turbine with four mooring lines (Sethuraman and Venugopal, 2013). In 2016, a 1:50 scaled model test of a 5 MW OC3 spar-type floating wind turbine which is designed for a water depth of 200 m was carried out at Shanghai Jiao Tong University. The dynamic responses in different sea conditions were recorded (Duan et al., 2016) and the research in this work is based on the correlative testing results.

This work studies the dynamic responses of the 5 MW OC3 spar-type floating wind turbine in different sea conditions through numerical calculations using fully coupled time domain FAST code (Jonkman and Jr, 2005). The numerical results are also validated by model tests. Also, the differences between them are discussed and the reasons are analyzed. It is expected that this study can bring valuable information for engineering application in the future.

2. Coupled dynamic analysis theory

Considering the rotation effect of blades, floating wind turbine is not only impacted by wave forces, but also wind loads. It is a blades-nacelle-tower-platform nonlinear coupled system and should be analyzed in time domain, which is different from the traditional offshore structures calculated by linear theories and methods.

In order to study the dynamic responses of floating wind turbine in time domain, the platform can be regarded as a rigid body and the motion equation of it can be given as:

$$(\boldsymbol{M}+\boldsymbol{A})\ddot{\boldsymbol{X}}(t)+\boldsymbol{C}\dot{\boldsymbol{X}}(t)+\boldsymbol{K}\boldsymbol{X}(t)=\boldsymbol{F}^{\text{waves}}(t)+\boldsymbol{F}^{\text{wind}}(t)+\boldsymbol{F}^{\text{mooring}}(t)+\boldsymbol{F}^{\text{vis}}(t) \tag{1}$$

Where $\boldsymbol{X}(t)$ is generalized displacement of the platform in time domain. $\dot{\boldsymbol{X}}(t)$ and $\ddot{\boldsymbol{X}}(t)$ are generalized velocity and acceleration respectively. $\boldsymbol{M}$ is mass matrix. $\boldsymbol{A}$ and $\boldsymbol{C}$ are added mass matrix and damping coefficient matrix, which are caused by wave radiation and can be calculated by WAMIT (Lee, 2013). $\boldsymbol{K}$ is hydrostatic restoring force matrix, which can also be calculated by WAMIT. $\boldsymbol{F}^{\text{waves}}(t)$ is incident-wave induced force. $\boldsymbol{F}^{\text{wind}}(t)$ is to present wind loads acting on blades and tower. $\boldsymbol{F}^{\text{mooring}}(t)$ is mooring tension, while $\boldsymbol{F}^{\text{vis}}(t)$ is drag force caused by fluid viscidity.

Wave induced force in frequency domain predicted by WAMIT based on potential flow theory will be transformed to load in time domain $\boldsymbol{F}^{\text{waves}}(t)$ by FAST. The load in the j^{th} direction can be calculated as (Jonkman and Sclavounos, 2006):

$$\boldsymbol{F}_j^{\text{waves}}(t)=\frac{1}{2\pi}\int_{-\infty}^{\infty}W(\omega)\sqrt{2\pi S_\zeta(\omega)}X_j(\omega,\beta)e^{-i\omega t}d\omega \tag{2}$$

Where ω is frequency of incident wave, $W(\omega)$ is the Fourier transform of a realization of a White Gaussian Noise time series process with unit variance, $S_\zeta(\omega)$ is two-sided wave spectrum which depends on ω. $X_j(\omega,\beta)$ is a wave induced force array normalized per unit wave amplitude, which depends on the geometry of the floating platform, frequency ω and direction of the incident wave β.

The aerodynamic load on blades is regarded as external load acting on the platform and can be calculated by blade element momentum theory (Hansen, 2008), the normal force and the torque on the control volume of thickness $d\boldsymbol{r}$ are:

$$d\boldsymbol{T}=\frac{1}{2}\rho BC_n\boldsymbol{V}_1^2(1-a)^2\cdot c\cdot\frac{d\boldsymbol{r}}{\sin^2\varphi} \tag{3}$$

$$d\boldsymbol{M}=\frac{1}{2}\rho BC_t\boldsymbol{V}_1(1-a)\omega\boldsymbol{r}(1+a')\cdot c\cdot\frac{\boldsymbol{r}d\boldsymbol{r}}{\sin\varphi\cos\varphi} \tag{4}$$

Where ρ is the air density, B is the number of blades, $\boldsymbol{V}_1$ is the wind speed, c is the chord of the airfoil, φ is the relation flow angle which equals the blades twist θ adding the angle of attack α, C_n and C_t are the coefficients for the normal force and thrust force which can be calculated by lift coefficient C_l and drag coefficient C_d ,respectively:

$$C_n = C_l \cos\varphi + C_d \sin\varphi \tag{5}$$

$$C_t = C_l \sin\varphi - C_d \cos\varphi \tag{6}$$

a and a' are the axial induction factor and the tangential induction factor, respectively. They can be calculated as the follows:

$$a = \frac{1}{\frac{4\sin^2\varphi}{\sigma C_n} + 1} \tag{7}$$

$$a' = \frac{1}{\frac{4\sin\varphi\cos\varphi}{\sigma C_t} - 1} \tag{8}$$

Where σ is the fraction of the annular area in a control volume.

$\boldsymbol{F}^{\text{mooring}}(t)$ is regarded as another external load, which can be divided into vertical tension V_F and horizontal tension H_F. They are solved by catenary equation using iteration method. Considering no section of the mooring line rests on the seabed, V_F and H_F can be analyzed as the follows (Jonkman, 2009b):

$$x_F(H_F, V_F) = \frac{H_F}{w}\left\{\ln\left[\frac{V_F}{H_F} + \sqrt{1+\left(\frac{V_F}{H_F}\right)^2}\right] - \ln\left[\frac{V_F - wL}{H_F} + \sqrt{1+\left(\frac{V_F - wL}{H_F}\right)^2}\right]\right\} + \frac{H_F L}{EA} \tag{9}$$

$$z_F(H_F, V_F) = \frac{H_F}{w}\left[\sqrt{1+\left(\frac{V_F}{H_F}\right)^2} - \sqrt{1+\left(\frac{V_F - wL}{H_F}\right)^2}\right] + \frac{1}{EA}\left(V_F L - \frac{wL^2}{2}\right) \tag{10}$$

Where x_F and z_F are respectively the horizontal and vertical coordinates of fairlead position relative to the anchor, w is the mass of mooring line per unit length, L is unstretched length of the total mooring line, and EA is the sectional stiffness of mooring line.

Besides, the flow separation behind cylindrical structures will induce viscous drag force. It can be estimated by Morison Equation:

$$\mathrm{d}\boldsymbol{F}_i^{\text{vis}} = \frac{1}{2}\rho C_{\mathrm{D}} D \mathrm{d}z \cdot \left(\boldsymbol{v}_{\mathbf{w},i} - \boldsymbol{v}_{\mathbf{s},i}\right)\left|\boldsymbol{v}_{\mathbf{w},i} - \boldsymbol{v}_{\mathbf{s},i}\right| \tag{11}$$

Where C_{D} is viscosity coefficient, $\boldsymbol{v}_{\mathbf{w},i}$ is the velocity of water and $\boldsymbol{v}_{\mathbf{s},i}$ is the velocity of strip.

3. The 5 MW OC3 spar-type floating wind turbine and cases definitions

3.1 Model test introduction

The 5 MW OC3 spar-type floating wind turbine is based on OC3-Hywind and it is modified to fit 200 m water depth. The taut mooring system is connected by a delta connection. The results used in this paper are based on a 1:50 scaled model test conducted at Shanghai Jiao Tong University. More details of the test can be found in the paper of Duan (2016). The main parameters are listed in Table 1, in which the negative sign indicates an elevation below the still water line.

Table 1 Main parameters of the floating wind turbine system

Item	Parameters
Rating	5 MW
Rotor orientation, Configuration	Upwind, 3 Blades
Rotor, Hub diameter	126 m, 3 m
Hub height	90 m
Blade length	61.5 m
Overhang	5 m
Rated wind speed	11.4 m/s
Platform length	130 m
Platform mass	7,316,578 kg

Platform CM(along the centerline of the platform)	-94.1495 m
Number of mooring lines	3
Angle between adjacent lines	120 deg
Angle between adjacent lines	1.22×10^{8} N
Entire floating wind turbine system mass	8,066,109 kg
Overall CM(along the centerline of the platform)	-78.947
Draft	120 m

3.2 Simulation model

The simulation model of the whole floating wind turbine system can be divided into five modules in FAST, i.e. aerodynamic module, structural dynamic module, hydrodynamic module, mooring module and control module. Each module are calculated independently and coupled by equivalent additional mass and load.

Blade element momentum theory considering dynamic stall is applied in aerodynamic module. Multi-body-dynamics formulation and FEM are used in structural dynamic module. Quasi-static catenary equation is applied in mooring module. In hydrodynamic module, hydrostatic restoring force, added mass and linear damping caused by wave radiation, wave exciting force, and drag force are considered. Hydrostatic restoring force, added mass and linear damping, as well as wave exciting can be solved and output in frequency domain by WAMIT based on potential flow theory. Then, the output of WAMIT will be used as the input for FAST. The panel model of the spar-type platform below waterline built in WAMIT is shown as Fig.1. Control module is imported to simulation in the form of a dynamic link library (DLL) to adjust the generator torque and blade pitch angle.

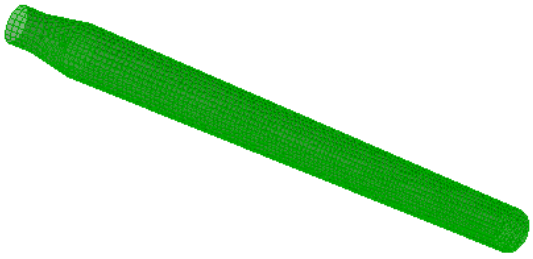

Fig.1 Panel model of the spar-type platform in WAMIT

3.3 Cases definitions

In order to study the dynamic response of the spar-type floating wind turbine, several cases showed in Table 2 are conducted. In which, the cases with steady wind only (LC1-LC3), steady wind combined irregular waves (LC4-LC6) and the combination of steady wind, irregular waves and current (LC7-LC9), free decay in still water (LC10) are included. The prototype wind speeds vary from the rated speed 11.4 m/s to speed 23 m/s. The prototype irregular wave is one-year return period irregular wave. For which, the significant wave height H_s is 7.1 m, spectral peak wave period T_p is 12 s and spectral peak parameter γ is 2.2. The current speeds vary from 0.50 m/s to 1.20 m/s.

Table 2 Cases definition

Load case	Wind speed (m/s)	H_s (m)	T_p (s)	γ	Current speed (m/s)
LC1	11.4	—	—	—	—
LC2	18	—	—	—	—
LC3	23	—	—	—	—
LC4	11.4	7.1	12.1	2.2	—
LC5	18	7.1	12.1	2.2	—
LC6	23	7.1	12.1	2.2	—
LC7	11.4	7.1	12.1	2.2	0.50
LC8	18	7.1	12.1	2.2	0.85
LC9	23	7.1	12.1	2.2	1.20

LC10	-	-	-	-	-

3.4 Assumptions for model test and simulation

In the model test, the Froude similarity rule is selected to scale the environment and the experimental model. Additionally, the scale effect caused by dissimilarity of Reynolds number has been revised. Assuming the lift coefficient and resistance coefficient of the blade airfoil are insensitive to Reynolds number, tip speed ration similarity is adopted. In the model test, active wave elimination device is installed on both sides of the basin, so reflection effect of wave is regarded as non-existent. More importantly, the quality of wind field determines the aerodynamic load whether or not accurate. To guarantee the wind environment quality for steady wind speeds, a wind generation system which is consisted of 9 independently controllable axial fans in a 3×3 stacked square configuration is applied and a honeycomb screen is attached to the front of the wind generation system.

In numerical simulation, it is assumed that the floating support platform is a six-DOF rigid body with three small rotational displacements and the tower is rigidly cantilevered to the support platform. The blades and tower are regarded as flexible body and can be characterized using a linear modal by assuming small deflections within each member. In hydrodynamics module, the linearization assumption of the classical marine hydrodynamics is adopted and viscous-drag term is considered by Morison Equation. In mooring module, the dynamic part of mooring lines is ignored and the drag force acting on the mooring lines is neglected. Moreover, the delta connection is ignored. More details can be found in the paper of Jonkman J.M. (2007).

4. Results comparison and discussion

4.1 Free decay

Comparing the free decay results from numerical calculation and model test can verify both methods preliminarily. From Table 3, it can be found that the results from numerical calculation and model test match well.

Table 3 Free decay results of main freedoms

Item	Surge		Pitch		Heave		Yaw	
	Model Test	Numerical Calculation	Model Test	Numerical Calculation	Model Test	Numerical Calculation	Model Test	Numerical Calculation
Natural period (s)	40.47	40.43	33.94	33.83	27.54	27.65	5.95	5.96
Damping ratio	0.038	0.047	0.035	0.015	0.028	0.027	0.086	0.072

4.2 Surge, pitch and heave motions

The surge and pitch responses of the platform are obvious motion modes of the whole system. Wind, wave and current have different effects on surge and pitch. Comparisons are conducted by statistics in time domain and shown in Table 4. From where it can be found that when wind speed is increasing over the rated speed, the responses of surge and pitch reduce with the decreasing of axial thrust. Besides, the average responses of surge and pitch change observably with wind speed changing. Comparing the wind only load cases (LC1-LC3) with wind-wave cases (L4-LC6), it can be found that the average responses of surge and pitch change lightly, but the fluctuation amplitudes of surge and pitch vary greatly. Take the surge responses in model tests for example, the average responses for LC1 and LC4 are respectively 8.67 m and 8.68 m, which are similar to each other. However, the fluctuation amplitude for LC1 is 1.73 m while that for LC4 is 8.23 m with the effect of wave. Comparing the wind-wave cases (LC4-LC6) with the combination of wind, wave and current load cases (LC7-LC9), it is found that current increases the average response, but has little influence on motion fluctuation amplitude. Also, take the surge responses in model tests for example, the average response for LC4 is 8.68 m, while it adds to 9.24 m with the effect of current. Thus, the average responses of surge and pitch are mainly induced by wind, while the current will magnify the effect of induction. But the amplitude of surge and pitch are mostly dominated by wave.

Considering the results from numerical calculations and model tests, take the surge response for LC1 for example, the fluctuation amplitude of model test is 1.73 m, while that of numerical calculation is only 0.11 m. Also, it can be found that the fluctuation amplitudes of numerical calculations in other load cases are smaller than those of model tests. The smaller fluctuation amplitude of numerical calculation is mainly due to less accounting

for the instability of wind and this phenomenon is particularly obvious with wind only. The average response of numerical calculation is bigger than that of model test at rated wind speed 11.4 m/s, but is smaller than the model tests at 18 m/s and 23 m/s. The discrepancy is mainly due to the influence of modeling of mooring system. The catenary model of FAST hardly supplies the great mooring tension as taut mooring of model test in great deflection condition. When the wind speed reaches rated wind speed 11.4 m/s, the floating wind turbine will subject to a great wind load. With smaller restoring force supplied by mooring tension, the total environment load on the platform is greater. Thus, the deflection calculated by FAST is more than that of the model test. With the wind speed increasing, the total environment load and average response in simulation become smaller than that in model test.

Table 4 Statistics of surge and pitch in time domain

Response	Load case	FAST				Model test			
		Average	Max	Min	Amplitude	Average	Max	Min	Amplitude
Surge (m)	LC1	9.50	9.56	9.45	0.11	8.67	9.60	7.87	1.73
	LC2	5.05	5.12	4.97	0.15	6.04	6.72	5.44	1.28
	LC3	4.51	4.64	4.38	0.26	5.81	6.33	5.28	1.05
	LC4	8.97	12.34	4.73	7.61	8.68	13.48	5.25	8.23
	LC5	5.02	9.18	2.23	6.95	5.84	9.66	2.56	7.10
	LC6	4.49	8.74	1.81	6.93	5.82	9.67	2.55	7.12
	LC7	10.27	13.18	6.30	6.88	9.24	12.30	5.19	7.11
	LC8	8.46	11.62	4.96	6.66	7.11	11.24	3.74	7.50
	LC9	11.15	14.34	7.68	6.66	7.07	11.08	4.05	7.03
Pitch (deg)	LC1	6.52	6.55	6.50	0.05	6.00	6.72	5.47	1.25
	LC2	3.44	3.46	3.42	0.04	4.27	4.74	3.82	0.92
	LC3	3.07	3.09	3.05	0.04	4.14	4.54	3.71	0.83
	LC4	6.15	7.78	4.37	3.41	6.42	8.70	4.86	3.84
	LC5	3.42	5.33	1.99	3.34	4.52	6.27	2.82	3.45
	LC6	3.06	5.02	1.01	4.01	4.51	6.39	2.88	3.51
	LC7	6.43	8.00	4.69	3.31	6.49	8.40	4.47	3.93
	LC8	4.14	6.11	2.81	3.30	4.51	6.56	3.02	3.54
	LC9	4.38	5.87	2.78	3.09	4.37	6.22	2.87	3.35

Analyses also can be conducted in frequency domain. The left figures in Fig.2 and Fig.3 show power spectral density curves of surge and pitch respectively for FAST, while the right ones are for model test.

From the frequency response results of FAST and model test, it can be seen that both surge and pitch can be resolved into low frequency response and wave frequency response in a combination of wind, wave and current condition. Furthermore, the wave frequency response induced by wave plays a dominating role.

In Fig.2, it indicates that the peak of low frequency surge response of model test is at 0.154 rad/s, which is close to the natural frequency of surge at 0.155 rad/s. It proves that low frequency surge response is induced by natural frequency of surge. In Fig.3, it can be observed that the peak frequency of low frequency pitch response of model test is at 0.160 rad/s, which is lower than the natural frequency of pitch at 0.185 rad/s. Considering the natural frequency of surge is 0.155 rad/s, it indicates that pitch response is coupled with surge response.

From the power spectral density curves, it can be observed that the peaks of LC4 are higher than those of LC7 and the curves of LC1 are close to zero. It indicates that surge and pitch frequency responses are mainly induced by wave and will be restrained by wind and current. This is because wave has periodic characteristics and it will lead to periodic motions of surge and pitch, but wind and current loads are regarded as constant external forces and they will restrain the periodic motions of surge and pitch.

Though the general regularities for FAST and model test are similar, the power spectral density curves for FAST and model test show noticeable differences. FAST underestimates the frequencies of surge and pitch low frequency responses. This phenomenon is believed to be caused by unsteadiness of wind turbine system in simulations. Besides, the peaks in different load cases calculated by FAST are higher than those calculated by model test. The difference can be attributed to aero-damping.

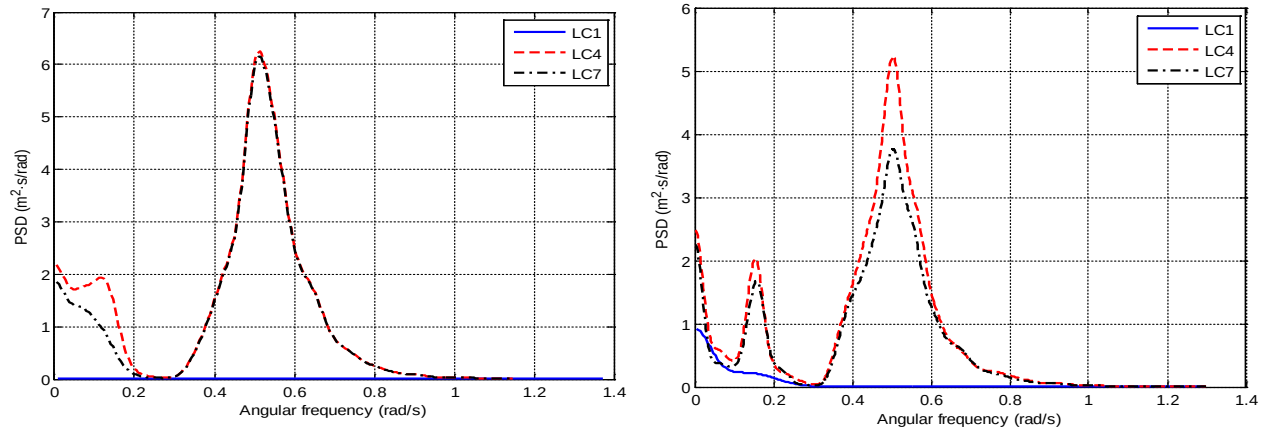

(a) FAST (b) Model test

Fig.2 Power spectral density curves of surge for FAST and model test

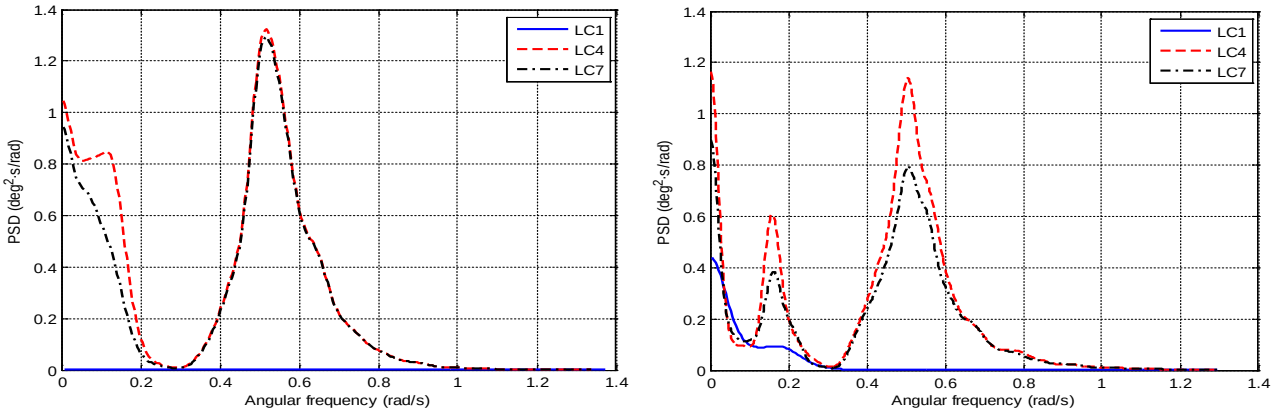

(a) FAST (b) Model test

Fig.3 Power spectral density curves of pitch for FAST and model test

Heave is another important motion response of the platform. From Table 5, it can be found that the average responses of heave will noticeably reduce with the increase of wind speed, but the fluctuation amplitudes will not change much with wind speed variations.

Table 5 Statistics of heave in time domain

Load case	FAST				Model test			
	Average (m)	Max (m)	Min (m)	Amplitude (m)	Average (m)	Max (m)	Min (m)	Amplitude (m)
LC4	-0.446	0.419	-1.103	1.522	-0.595	0.481	-1.794	2.275
LC5	-0.190	0.733	-0.798	1.531	-0.468	0.676	-1.581	2.257
LC6	-0.135	0.797	-0.757	1.554	-0.468	0.632	-1.563	2.195

Fig.4 shows that heave frequency response can also be resolved into low frequency response and wave frequency response in a combination of wind and wave condition. The peak of low frequency response appears at 0.226 rad/s, which is exactly the natural frequency of heave and far away from the natural frequencies of surge and pitch. Thus, it can be concluded that heave is not coupled with surge or pitch.

Also, it can be seen that the peak values for FAST and model test at the heave natural frequency differ greatly. The higher peak at heave natural frequency of model test shows heave response is affected greatly not only by wave frequency, but also by its natural frequency. The model test conducted in MARIN (Kimball et al.,

2012) also shows the similar result. But the lower peak of numerical calculation at natural frequency indicates that heave response is mainly affected by wave frequency. The discrepancy of FAST can be attributed to two main reasons. One of which is the different mooring system models. For catenary mooring system simulations, mooring tension has little effect on heave response. However, the mooring tension of the taut mooring system in model tests is comparatively bigger, and affects heave observably in the wind-wave conditions. On the other hand, for the wind field in model test is not perfectly steady, the low-frequency turbulent wind loads may increase the low frequency resonance response.

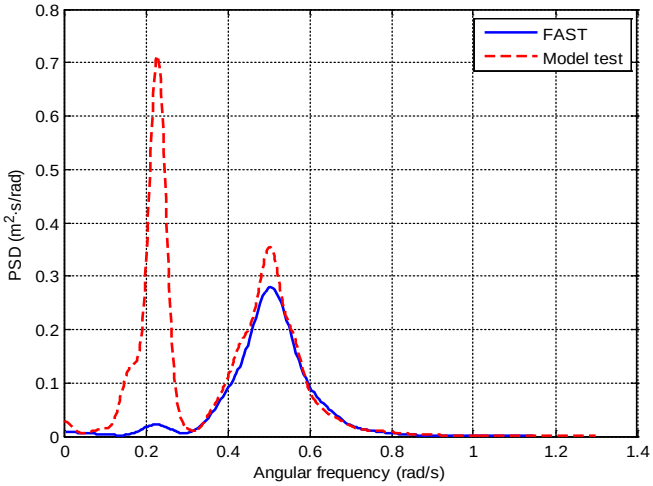

Fig.4 Power spectral density curves of heave for LC4

4.3 Yaw and tower top bending moment

Being different from traditional floating platforms, yaw of floating turbines is mainly caused by rotor rotations. The responses of the whole floating wind turbine system are closely related to yaw. Furthermore, tower top bending moment is mainly induced by yaw.

Fig.5 is the free decay of yaw (LC10). It can be seen the free decay curve from numerical calculation in time domain almost coincides with that from model tests, indicating that FAST can simulate free decay of yaw response well.

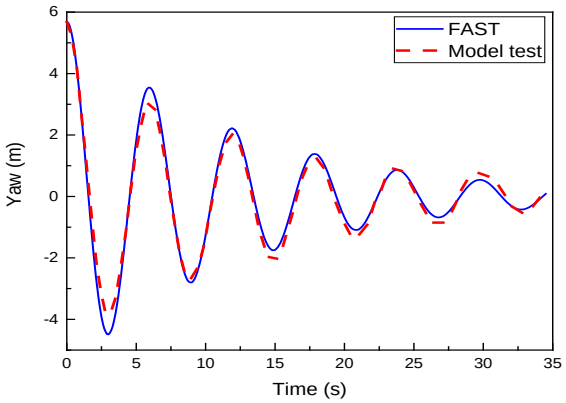

Fig.5 Free decay of yaw

Fig.6 shows the yaw and tower top bending moment responses of LC4 in time domain. It can be seen that the response of yaw from numerical calculations is small, which is differ greatly from the result from model tests. Also, the response of tower top bending moment from numerical calculations is far smaller than from model tests. This means FAST has limitation on simulating yaw and tower top bending moment in wind-wave conditions.

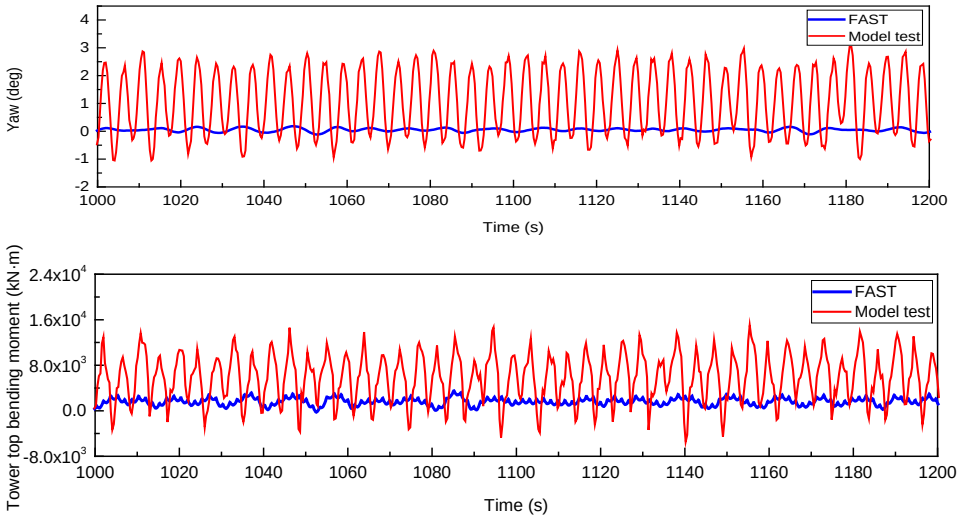

Fig.6 Yaw and tower top bending moment of LC4 in time history

Fig.7 is the power spectral density curves of yaw and tower top bending moment for LC4. Fig.7 (a) is for yaw and Fig.7 (b) is for tower top bending moment.

The spectrum of yaw in model test has two peaks. One peak is at 0.5 rad/s, which is induced by incident wave. The other peak is at high frequency 1.45 rad/s. The peak at wave frequency almost can be ignored compared to the peak at high frequency. Additionally, considering 1.45 rad/s is close to the rotation frequency 1.51 rad/s (Duan et al., 2016), it can be concluded that yaw is mainly induced by rotor rotation. The deviation between 1.45 rad/s and 1.51 rad/s may because the rotor speed does not speed up 14.4 rpm for the actual wind velocity may less than 11.4 m/s in the model test.

Similarly, tower top bending moment is mainly induced by rotor rotation as well. However, the spectra for FAST are different from the spectra for model tests, which have no peak at 1.45 rad/s. The reason for this deviation may due to the reason that FAST might have some limitations on simulating yaw and tower top bending moment in wind-wave conditions. Nevertheless, it can also be the modeling reason for the simulation of yaw rigidity in the model test, which proves the importance of simulating yaw rigidity through delta lines deploying way. Therefore, it is needed to make further investigation on the yaw stiffness simulation.

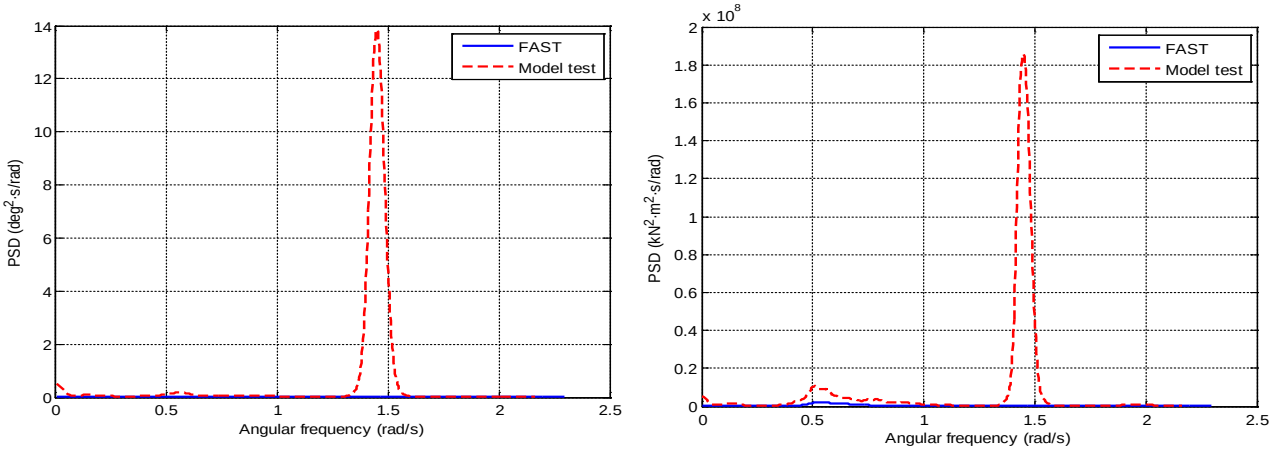

(a) Yaw (b) Tower top bending moment

Fig.7 Power spectral density curves of yaw and tower top bending moment

4.4 Mooring system response

Mooring tension is considered as an external load acting on the platform, which has an important effect on

the responses of the whole floating wind turbine system. Choose the mooring line along the wind direction as the research subject. Analyses are conducted by power spectral density curves which as plotted in Fig.8.

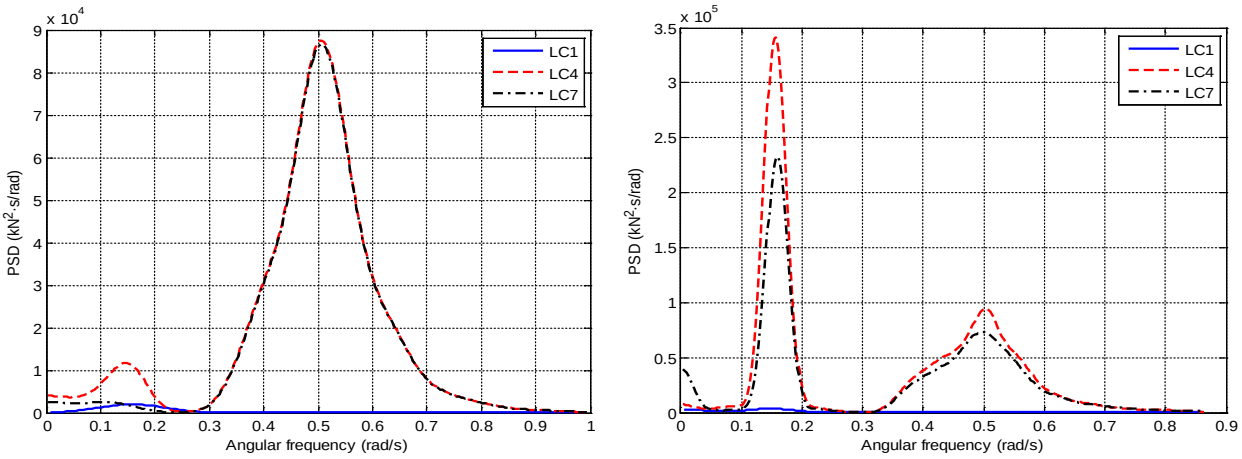

(a) FAST (b) Model test

Fig.8 Power spectral density curves of mooring tension for FAST and model test

Fig.8 (a) is the spectrum from FAST and Fig.8 (b) is the spectrum from model test. There is a distinct peak at 0.51 rad/s for both FAST and model test. Consider the irregular wave spectrum peak period is 12.1 s, meaning that the frequency of incident wave is 0.52 rad/s. Thus, the peak at 0.51 rad/s is mainly induced by incident wave. There is another peak at 0.156 rad/s, which can be regarded as the resonant frequency corresponding to natural frequency of some motion of the floating wind turbine system. But the peaks of LC1, LC4 and LC7 at natural frequency for FAST are smaller than those for model test. This phenomenon is similar to the heave responses for similar reasons as analyzed above.

Besides, it can be found that 0.156 rad/s is nearly the same with the natural frequency of surge 0.155 rad/s, which indicates that surge has an obvious coupling effect on the dynamic response of the mooring system in wave or wind-wave conditions.

4.5 Rotor thrust and tower top shear force

Rotor thrust is related closely to the whole floating wind turbine system and the tower top shear force influences the structural safety greatly, the study of rotor thrust and tower top shear force in different conditions is of crucial importance. The average values of rotor thrust and tower top shear force in time domain are summarized in Table 6.

From Table 6, it can be found that he numerical results show similar tends as the results of model test. Rotor thrust and tower top shear force will reach the maximal values at 11.4 m/s and will decrease with wind speed increase. This indicates that the area of blades exposed to wind will decrease with wind speeding up and the axial thrust will consequently decrease. From Table 6, it also can be found that the average values of rotor thrust and tower top shear force in the combination of wind and irregular wave conditions (LC4-LC6) are smaller than those in wind only conditions (LC1-LC3). Considering the rated power reached at higher wind speed in the combination of wind and wave condition, it indicates that the average relative velocity of incident wind will decrease under the periodic action of wave.

Besides, the results from FAST are always smaller than the values given by model tests. The rotor thrust calculated does not contain the rotor thrust acting on the hub only, but also the inertial force acting on it. Thus, the discrepancy is mainly consisted of two parts. On one hand, the angle between incident wind and shaft will cause a relative wind speed decrease, which will reduce the rotor thrust acting on the hub. On the other hand, pitch angles in simulation are smaller than those in model test, which will reduce the rotor thrust acting on the hub calculated by FAST even further.

Table 6 Average values of rotor thrust and tower top shear force in time domain

Load case	FAST		Model test	
	Rotor thrust(kN)	Tower top shear force (kN)	Rotor thrust(kN)	Tower top shear force (kN)
LC1	923	1120	978	1217
LC2	517	579	657	836
LC3	443	490	627	804
LC4	877	1058	904	1190
LC5	513	574	585	795
LC6	442	488	578	787
LC7	884	1077	933	1208
LC8	528	619	716	894
LC9	467	569	681	846

In order to compare the results of numerical calculation and model test, power spectral density curves are plotted in Fig.9. The power spectral density curves of model test have five peaks for wind-wave condition and the reasons causing these five peaks have been explained in the paper of Duan (2016): The first peak is caused by unsteadiness of wind generation system, the second peak is induced by incident wave, the third peak is caused by rotor rotation, the fourth peak is induced by the first-mode tower vibration and the fifth appears near the 3P frequency. But the curves of numerical calculation for wind-wave condition only have two spectral peaks. One peak is caused by unsteadiness of wind generation system, while the other is induced by incident wave. It indicates that FAST has limitations on simulating the responses of rotor thrust and tower top shear force induced by the vibration of tower and the rotation of rotor. On contrast, the peaks of FAST and model test at wave frequency match well, which indicates FAST can simulate the responses of rotor thrust and tower top shear force induced by wave well. Besides, from Fig.9, it can be found that the peaks induced by wave is far higher than the others, which means rotor thrust and tower top shear are both mainly influenced by wave.

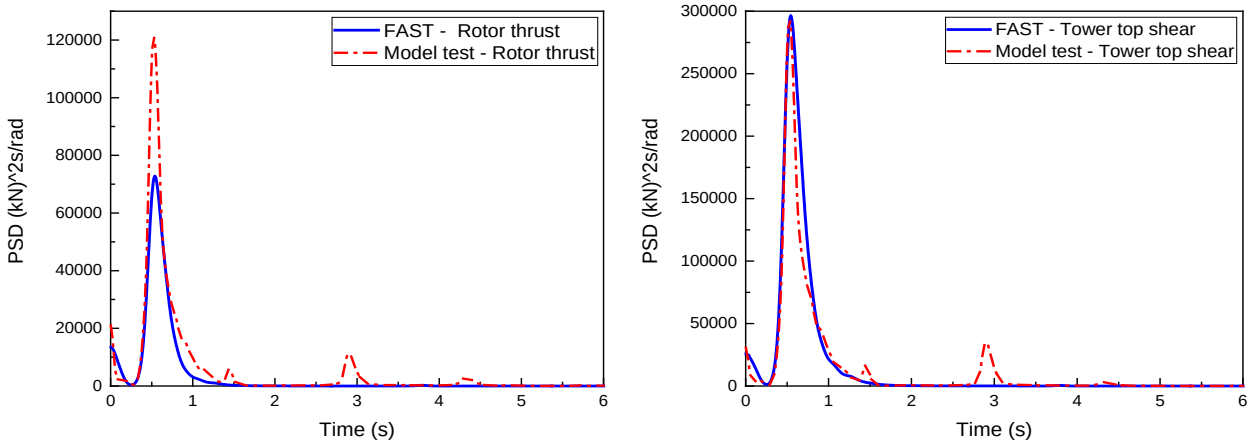

Fig.9 Power spectral density curves of rotor thrust and tower top shear force for LC4

5. Conclusions

In this paper, dynamic response of a 5 MW OC3 spar-type floating wind turbine in different conditions is analyzed in both time domain and frequency domain by FAST code and a 1:50 scaled model test. The discrepancies between numerical calculations and model tests are compared and discussed. Several conclusions can be drawn as the follows.

On the basis of the comparisons of numerical calculation and model test, it can be found that the results of FAST are credible in general. However, there are some discrepancies between the results of FAST and model test as well. Though yaw responses in free decay for FAST and model test match well, there is a noticeable gap between them in wind-wave conditions. Compared to model test, FAST will underestimate the impact of low frequency on heave and mooring tension and it has limitation on simulating the responses of rotor thrust and tower top shear force induced by the vibration of tower and the rotation of rotor.

According to the comparisons of numerical calculation and model test, several motion characteristics are

concluded. Surge and pitch are coupled with mooring tension, but heave is independent from them. Surge, pitch, rotor thrust and tower top shear force are mainly induced by wave in wind-wave conditions, but yaw and tower top bending moment are mainly induced by rotor rotation.

Besides, the impacts of wind, wave and current on responses are also discussed. Wind and current will induce the low-frequency average responses, while wave will induce the fluctuation amplitudes of responses. Besides, wave will induce wave-frequency responses, but wind and current will restrain the amplitudes of the responses.

Acknowledgement

This work is financially supported by the State Key Laboratory of Ocean Engineering in Shanghai Jiao Tong University and National Key R & D Project (Grant NO.2016ZX05028-002-004). These supports are greatly appreciated by the authors.

References

Chen J.H., Hu Z.Q. and Liu G.L., 2017. Investigation on high-order coupled rigid-flexible multi-body dynamic code for offshore floating wind turbines. *Proc. of ASME 36th International Conference on Ocean, Offshore and Arctic Engineering*, Trondheim, Norway.

Duan F., Hu Z.Q. and Niedzwecki J.M., 2016. Model test investigation of a spar floating wind turbine. *Marine Structures*, **49**:76-96.

Goupee A.J., Koo B., Kimball R W., Lambrakos K.F. and Dagher H.J., 2012. Experimental comparison of three floating wind turbine concepts. *Proc. of ASME 31st International Conference on Ocean, Offshore and Arctic Engineering*, Rio de Janeiro, Brazil.

Hansen M.O.L, 2008. *Aerodynamics of wind turbines*, London, UK, Earthscan.

Jonkman J., Butterfield S., Musial W. and Scott G., 2009. Definition of a 5-MW reference wind turbine for offshore system development. *Technical Report NREL/TP-500-38060*, Colorado.

Jonkman J., 2009. Dynamics of offshore floating wind turbines-Model development and verification. *Wind Energy*, **12** (5): 459-492.

Jonkman J., 2010. Definition of the floating system for phase Ⅳx of OC3. *Technical Report NREL/TP-500-47535*, Colorado.

Jonkman J.M. and Jr B.M.L.,2005. FAST user's guide. *Technical Report NREL/EL-500-38230*, Colorado.

Jonkman J.M. and Sclavounos P.D., 2006. Development of fully coupled aeroelastic and hydrodynamic models for offshore wind turbines. *Proc. of ASME Wind Energy Symposium*, Reno, Nevada, USA.

Jonkman J.M., 2007. Dynamics modeling and loads analysis of an offshore floating wind turbine. *Technical Report NREL/TP-500-41958*, Colorado.

Jonkman J.M., Larsen T., Hansen A., Nygaard T., Maus K., et al., 2010. Offshore code comparison collaboration within IEA wind task 23: Phase IV results regarding floating wind turbine modeling. *European Wind Energy Conference (EWEC)*, Warsaw, Poland.

Karimirad M. and Moan T., 2012. Wave- and wind-induced dynamic response of a spar-type offshore wind turbine. *Journal of Waterway Port Coastal and Ocean Engineering*, **138**(1):9-20.

Kimball R.W., Goupee A.J., Coulling A.J. and Dahger H.J., 2012. Model test comparisons of TLP, spar-buoy and semi-submersible floating offshore wind turbine systems. *Proc. of Society of Naval Architects & Marine Engineers*, Providence, Rhode Island, USA.

Kimball R.W., Goupee A.J., Fowler M.J., Ridder E.J.D. and Helder J., 2014. Wind/wave basin verification of a performance-matched scale-model wind turbine on a floating offshore wind turbine platform. *Proc. of ASME 33rd International Conference on Ocean, Offshore and Arctic Engineering*, San Francisco, California, USA.

Koo B., Goupee A.J., Lambrakos K. and Kimball R.W., 2012. Model tests for a floating wind turbine on three different floaters. *Proc. of ASME 31st International Conference on Ocean, Offshore and Arctic Engineering*, Rio de Janeiro, Brazil.

Koo B., Goupee A.J., Lambrakos K. and Lim H.J., 2013. Model test correlation study for a floating wind turbine on a tension leg platform. *Proc. of ASME 32nd International Conference on Ocean, Offshore and Arctic Engineering*, Nantes, France.

Kvittem M.I., Bachynski E.E. and Moan T., 2012. Effects of hydrodynamic modelling in fully coupled simulations of a semi-submersible wind turbine. *Energy Procedia*, **24**:351-362.

Lee C., 2013. WAMIT theory manual. *http://www.wamit.com.*

Martin H.R., Kimball R.W., Viselli A.M. and Goupee A.J., 2012. Methodology for wind/wave basin testing of offshore floating wind turbines. *Proc. of ASME 31st International Conference on Ocean, Offshore and Arctic Engineering*, Rio de Janeiro, Brazil.

Muliawan M.J., Karimirad M., Gao Z. and Moan T., 2013. Extreme responses of a combined spar-type floating wind turbine and floating wave energy converter (STC) system with survival modes. *Ocean Engineering*, **65**(2):71-82.

Nielsen F.G., Hanson T.D. and Skaare B., 2006. Integrated dynamic analysis of floating offshore wind turbines. *Proc. of ASME 25th International Conference on Offshore Mechanics and Arctic Engineering*, Hamburg, Germany, 671-679.

Ridder E.D., Otto W., Zondervan G., Huijs F. and Vaz G., 2014. Development of a scaled-down floating wind turbine for offshore basin testing. *Proc. of ASME 33rd International Conference on Ocean, Offshore and Arctic Engineering*, San Francisco, California, USA.

Robertson A., Jonkman J., Masciola M, Song H., Goupee A. Coulling A. and Luan C., 2014. Definition of the semisubmersible floating system for phase II of OC4. *Technical Report NREL/TP-5000-60601*, Colorado.

Sethuraman L. and Venugopal V., 2013. Hydrodynamic response of a stepped-spar floating wind turbine: Numerical modelling and

tank testing. *Renewable Energy*, **52**: 160-174.
Thomas S., 2010. *Dynamic response analysis of a spar type floating wind turbines*, Master's thesis, Trondheim: Norwegian University of Science and Technology.